⌘ *Author's Choice*

Yeast 18 S rRNA Is Directly Involved in the Ribosomal Response to Stringent AUG Selection during Translation Initiation*□S

Naoki Nemoto[‡1], **Chingakham Ranjit Singh**[‡1], **Tsuyoshi Udagawa**[‡1], **Suzhi Wang**[‡§1], **Elizabeth Thorson**[‡],
Zachery Winter[‡], **Takahiro Ohira**[‡], **Miki Ii**[‡], **Leoš Valášek**[¶], **Susan J. Brown**[‡§], and **Katsura Asano**[‡2]

From the ‡*Molecular Cellular and Developmental Biology Program and* §*Arthropod Genomics Center, Division of Biology, Kansas State University, Manhattan, Kansas 66506 and the* ¶*Laboratory of Regulation of Gene Expression, Institute of Microbiology, Academy of Sciences of the Czech Republic, Prague, Videnska 1083, 142 20, The Czech Republic*

In eukaryotes, the 40 S ribosomal subunit serves as the platform of initiation factor assembly, to place itself precisely on the AUG start codon. Structural arrangement of the 18 S rRNA determines the overall shape of the 40 S subunit. Here, we present genetic evaluation of yeast 18 S rRNA function using 10 point mutations altering the polysome profile. All the mutants reduce the abundance of the mutant 40 S, making it limiting for translation initiation. Two of the isolated mutations, *G875A*, altering the core of the platform domain that binds eIF1 and eIF2, and *A1193U*, changing the h31 loop located below the P-site tRNA$_i^{Met}$, show phenotypes indicating defective regulation of AUG selection. Evidence is provided that these mutations reduce the interaction with the components of the preinitiation complex, thereby inhibiting its function at different steps. These results indicate that the 18 S rRNA mutations impair the integrity of scanning-competent preinitiation complex, thereby altering the 40 S subunit response to stringent AUG selection. Interestingly, nine of the mutations alter the body/platform domains of 18 S rRNA, potentially affecting the bridges to the 60 S subunit, but they do not change the level of 18 S rRNA intermediates. Based on these results, we also discuss the mechanism of the selective degradation of the mutant 40 S subunits.

The translation reaction, or mRNA-dependent protein synthesis, is catalyzed by the ribosome, a large ribonucleoprotein complex, with assistance from translation factor proteins. During the initiation phase, the ribosome dissociates into the large (50 S in Bacteria and 60 S in Eukarya) and small (30 S in Bacteria and 40 S in Eukarya) subunits, and the latter binds the methionyl initiator tRNA (Met-tRNA$_i^{Met}$; its amino group is

formylated in Bacteria) and mRNA with the help of initiation factors (initiation factors for Bacteria and eIF for eukaryotic initiation factors) (reviewed in Refs. 1–3). As the consequence, the anticodon of the tRNA$_i^{Met}$ is base-paired to the start codon of the mRNA at the peptidyl-tRNA-binding site (P-site) of the small ribosomal subunit. The universally conserved factors, eIF1A/IF1 and eIF5B/IF2, are proposed to bind the small subunit at conserved locations and play distinct yet similar roles between Bacteria and Eukarya (4, 5).

The fidelity of start codon recognition is regulated by eIF1A/IF1 that binds the small subunit A-site (6, 7) as well as by other initiation factor(s) specific to each domain of life, IF3 in Bacteria (2) and eIF1, eIF2, eIF3, and eIF5, in Eukarya (eukaryotes). eIF2 is a heterotrimeric factor that binds Met-tRNA$_i^{Met}$ depending on a bound GTP. The resulting ternary complex (TC)[3] binds the 40 S subunit in the context of multifactor complex (MFC) with eIF1, -3, and -5, forming a 43 S preinitiation complex (PIC) (8). eIF1A also promotes TC loading onto the 40 S subunit (7). Start codon selection by PIC requires the eIF5-catalyzed GTP hydrolysis for eIF2 and is executed by a mechanism that involves the release of eIF1 and the resulting P$_i$, in response to AUG recognition (9). Subsequently, conformational changes in eIF2 allow it to leave the PIC together with eIF5. The clearance of at least eIF2 and eIF5 appears to be the requisite for subsequent 60 S subunit joining mediated by eIF5B (1, 3). In Archaea, aIF1 is a fidelity factor similar to eIF1 (10), in support of the phylogenetic relationship between Archaea and Eukarya, as proposed by Woese *et al.* (11).

X-ray crystallography of bacterial and archaeal ribosomes indicates that three-dimensional arrangement of rRNA determines the ribosome structure (reviewed in Ref. 12). Bacterial 16 S rRNA, as well as its eukaryotic counterpart, 18 S rRNA, contains 5′, central, 3′ major, and 3′ minor domains, which make up the body, platform, head, and a major projection from the body structure, respectively, of the small ribosomal subunit (see Fig. 1*A* for the secondary structure of yeast 18 S rRNA) (13). The larger mass of the eukaryotic 40 S subunit compared with the bacterial and archaeal 30 S subunit is partly due to

[3] The abbreviations used are: TC, ternary complex; MFC, multifactor complex; PIC, preinitiation complex; SSU, small subunit; uORF, on upstream ORF; 3AT, 3-aminotriazole; GMPPNP, guanosine-5′-[(β,γ)-imido]triphosphate; h, helix; hc, high copy; oligo, oligonucleotide; FOA, 5-fluoroorotic acid; P/M, polysome to monosome.
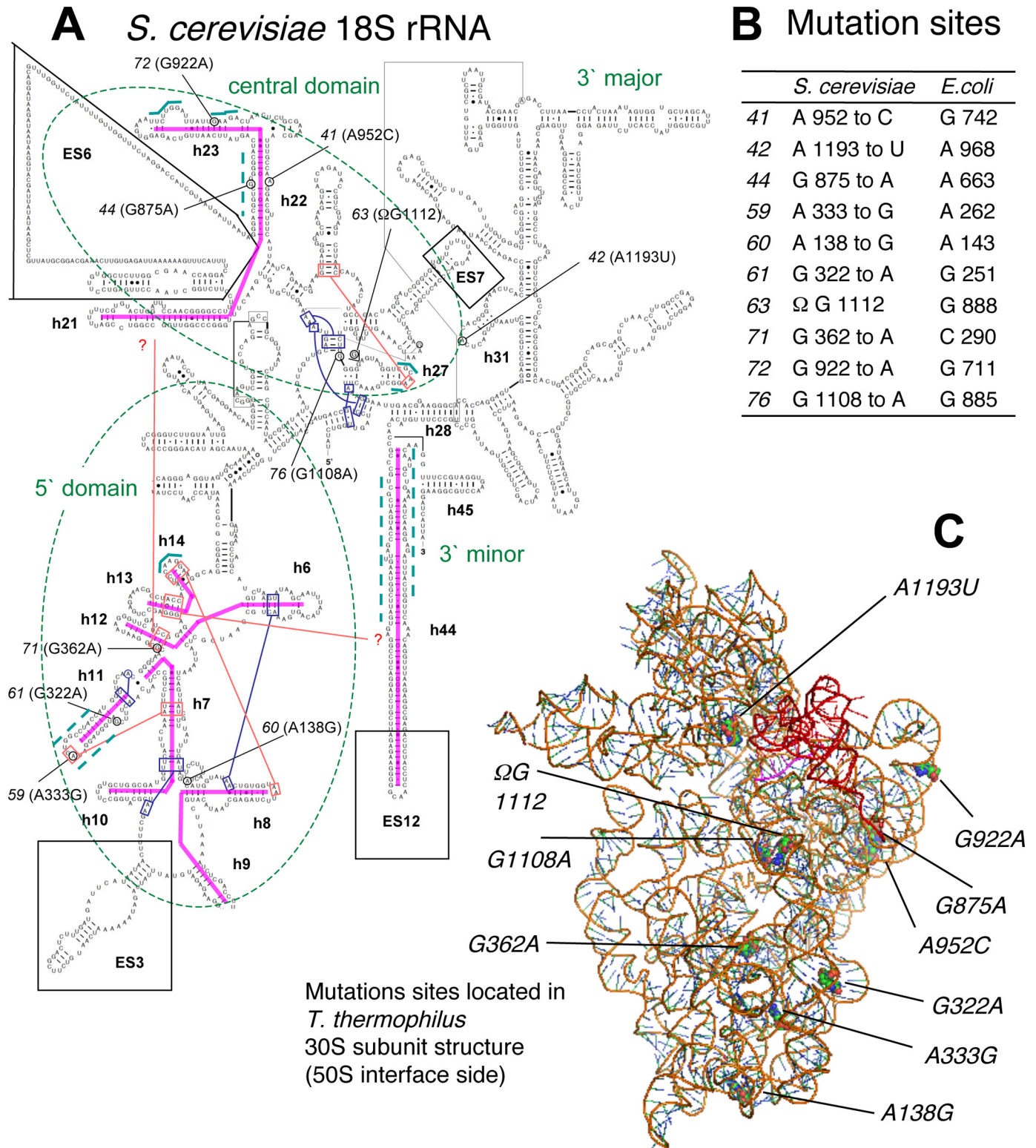
FIGURE 1. **Location of point mutations mapping in yeast 18 S rRNA.** *A*, mutation sites were identified in the predicted secondary structure of *S. cerevisiae* 18 S rRNA. *Pink thick lines* indicate five of the seven coaxially stacked helices (*i.e.* h6/h12, h8/9, h10/h7/h11-bottom, h11, and h13/h14), which are predicated from the homology to bacterial 30 S subunit structure. These seven stacked helices may be affected by mutations isolated in this study (see "Discussion"). The 18 S rRNA folds into four domains, with their names indicated by *thick letters* and with 5' and central domains, altered by 9 of the 10 isolated mutations, as indicated by *dotted circles*. *Thick blue lines* along the RNA sequence denote the predicted interface to the 60 S subunit, based on its homology to the structure of the bacterial ribosome (12) and cryo-EM structure of the eukaryotic one (15–17). *Boxed* are the expansion segments specific to eukaryotic rRNAs, numbered as in Ref. 14. *Blue* and *red thin lines* indicate A-minor interactions involving the bases *boxed* with the same color, either confirmed or predicted, respectively, in the bacterial 30 S subunit structure. *B*, mutations found in 10 isolated alleles are tabulated along with the corresponding *E. coli* residues. *C*, location of the altered bases is presented as space-filled in the *Thermus thermophilus* structure. *Yellow backbone* describes 18 S rRNA, whereas *red* and *pink backbones* denote P-site tRNA and mRNA, respectively. The schematics were constructed using PyMOL and Protein Data Bank code 2ow8. *Colors* of parts of the structures are shown more progressively faded when they are located more distant from the viewer.

several major expansion segments of 18 S rRNA inserted into the core rRNA sequence conserved between 16 S and 18 S rRNA (*boxes* in Fig. 1*A*) (14). Three-dimensional structure of the yeast and mammalian ribosomes have been predicted by fitting these additional segments to the portions of 40 S subunit cryo-EM structure, which could not be filled with the structure predicted with the bacterial 30 S subunit structure (15–18). Hydroxyl radical cleavage, cryo-EM, and other studies elucidated approximate locations of eIF1, eIF1A, eIF2α/γ, eIF3, eIF4G (the major adaptor subunit of eIF4F), and eIF5 on the 40 S subunit (reviewed in Ref. 19). In particular, eIF1 was linked to helix (h)23 and h24 of the central domain and h44 of the 3′ minor domain by hydroxyl radical cleavage (20). Cryo-EM studies support this location close to the E-site (6).

Within the yeast ribosomal DNA (*RDN*) repeat, the RNA polymerase I drives transcription of 35 S rRNA, the precursor for 18 S, 5.8 S, and 25 S rRNA, whereas RNA polymerase III drives 5 S rRNA transcription (supplemental Fig. S1) (reviewed in Ref. 21). In the nucleolus, 35 S rRNA is processed, modified, and assembled with ribosomal proteins, producing the 90 S preribosome, which is cleaved into large and small presubunits. They are then separately transported into the cytoplasm while maturing into the final products, the 40 S and 60 S subunits, containing 18 S rRNA and 25 S, 5.8 S, and 5 S rRNAs, respectively (21). The ribosomes misprocessed or those containing mutations are degraded (21). Different "nonfunctional" rRNA decay pathways that degrade mutant rRNA altering bases important in bacterial rRNAs have been identified (22–24).

The role of yeast 18 S rRNA in elongation and termination functions, as well as antibiotic resistance, has been extensively studied by site-directed mutagenesis of universally conserved residues important in bacterial 16 S rRNA (25–28), taking advantage of strains deleted for all ~100 *RDN* repeats but carrying a high copy (hc) *RDN* plasmid (29, 30). Recently, Dong *et al.* (31) identified by random mutagenesis that 18 S rRNA nucleotides in the h28 region are important for initiator tRNA binding and AUG selection. Here, we report the characterization of 10 18 S rRNA mutations obtained by screening for slow growth (Slg⁻) or temperature-sensitive (Ts⁻) mutants that alter the polyribosome (polysome) profile, indicative of changes in translation status in the cell. Our results extend the earlier report (31) and provide further evidence that the 18 S rRNA domains making up the decoding site and the eIF platform are directly involved in translation initiation, regulating the stringent selection of start codons.

MATERIALS AND METHODS

Plasmids and Yeast Strains—Plasmids and yeast strains carrying yeast *rdn* mutants are listed in Table 1. Other plasmids used include YCpU-SUI3 (*SUI3 URA3*) and YCpU-SUI3-2 (*SUI3-2 URA3*) (32) and modified *GCN4-lacZ* reporter plasmids pM199, pM226, and p227 (33, 34). pKA624 (*his4-306Δ URA3*) was generated by subcloning into pRS306 a DNA segment derived from PCR using a pair of *HIS4* oligos and p391 (34) as template, as described for a similar *his4Δ URA3* integration plasmid (32).

To prepare pNOY373 derivatives carrying *rdn-41a* and *rdn-59a* (Table 1, 6th column), we subcloned 2940-bp PstI-DraIII

fragment of pNOY373-41 and -59, respectively, into the same sites of pNOY373. We confirmed by sequencing that the *rdn-41b* and *rdn59b* mutations found in 25 S rRNA-coding region of the originally isolated plasmids were eliminated in the resulting plasmids.

KAY488 is a remake of NOY890 (30), derived from NOY908 (30) transformant carrying pRDN-hyg (*RDN*^hyg *URA3*). Because NOY890 was not available, we predominantly used KAY488 for plasmid shuffling in this study. Thus, the strain is referred to as NOY890 (KAY488) throughout the text. KAY165 (Table 1) was constructed by introducing *his4-306*(*TTG*) allele by transformation of NOY908 with an XhoI-linearized pKA624, followed by homologous recombination-mediated removal of *URA3* by selecting against Ura⁺. Details in our method of introduction of *HIS4* initiation codon mutations was described elsewhere (32). KAY171 was generated from a KAY165 transformant carrying pRDN-hyg. A Leu⁻ Ura⁺ progeny derived from the transformant was selected from its culture grown in the presence of leucine, designated KAY171, and used for plasmid shuffling.

Yeast rRNA Mutant Isolation—We mutagenized a pool of the hc *LEU2* plasmid pNOY373 encoding a wild-type rDNA repeat (supplemental Fig. S1) using a mutator *Escherichia coli* strain XL1-Red, and we used it to transform NOY890 (KAY488). We used the drug 5-fluoroorotic acid (FOA) as the reagent to select against the *URA3* plasmid (35); thus, the growth of the double plasmid transformants will produce only yeast derivatives bearing hc *LEU2* rDNA plasmid, unless the latter carries a lethal rDNA allele. The frequency of formation of FOA resistant cells from NOY890 (KAY488) transformants with a hc*LEU2* rDNA plasmid was lower at the regular temperature of 30 °C than in a typical plasmid shuffling done with commonly used yeast strains deleted for a protein factor, and even lower at a higher temperature of 36 °C. This prevented us from screening for Ts⁻ mutants simply by comparing the cell growth on FOA medium at 30 and 36 °C, as typically done to obtain protein factor mutations (36). Instead, we re-streaked FOA-resistant cells that had been grown at 30 °C onto two rich YPD plates and compared the growth between the two temperatures.

Sequence Analysis of the RDN Loci of pNOY373 Derivatives Bearing Ts⁻ or Slg⁻ Mutations—pNOY373 derivatives isolated from mutant candidates, as described in the text and Table 1, were sequenced using oligodeoxyribonucleotides listed in supplemental Table S1 and supplemental Fig. S1. Prior to determining the mutant sequences, we determined the sequence of the 9150-bp PstI-BamHI *RDN* insert of wild-type pNOY373 (GenBank™ accession number DQ888227), using the same set of oligos (see the structure of the *RDN* locus in supplemental Fig. S1). The chromatogram files of the sequences generated from the mutant plasmids were then analyzed using Mutation Surveyor® version 3.0 (Softgenetics LLC). This software allowed us to compare up to 24 different mutant chromatogram patterns at once, thereby unambiguously identifying mutation sites, including base deletion or insertion within a long stretch of the same nucleotide. The supplemental Table S2 indicates that all the 18 S rRNA mutants listed contained other mutations besides base changes within 18 S rRNA. To evaluate these non-18 S mutations, we performed systematic BLAST searches

using different *RDN* segment sequences as query, as described below.

Comparative Genomics Approaches—To examine evolutionary conservation of each of the *Saccharomyces cerevisiae* rRNA residues, we utilized a small or large subunit RNA variability map available on line (37, 38). These maps categorize every residue of SSU and large subunit rRNA according to the level of conservation throughout eukaryotes, and the map for *S. cerevisiae* SSU (18 S) rRNA was used in supplemental Fig. S2.

To examine polymorphisms within the *S. cerevisiae RDN* locus, we undertook systematic BLAST searches with each of the nine segments derived from the 9.15-kb pNOY373 insert sequence as listed across the top of supplemental Table S2. We wrote Perl scripts to parse BLAST hits that exceed a predefined cutoff score as follows: (i) a specified length in bp (longer than 300 bp), (ii) a specified probability score (less than $1\ e^{-1}$), and (iii) a specified identity (larger than 95%). rDNA sequences in the resulting hits were processed for multiple sequence alignment to identify polymorphisms among different *S. cerevisiae* strains/isolates or closely related *Saccharomyces* species. As a result, we identified 17 and 57 naturally occurring base changes (polymorphisms) within the *RDN* segment upstream of 18 S rRNA (supplemental Table S3) and the 18 S-coding region (supplemental Table S4), respectively (Polymorphisms found in the remaining *RDN* regions will be reported elsewhere.) The supplemental Table S5 summarizes variations at major T or A stretches found throughout the entire *RDN* locus during the searches. These results indicated that the remaining mutations found outside of 18 S rRNA (supplemental Table S2) are either a common polymorphism found at the site of consecutive A or T residues (supplemental Table S5) or a base change least likely to affect the production of the ribosome (see supplemental text for details).

Ribosome Analyses—Polysome profiling was performed by sucrose gradient velocity sedimentation of extracts of yeast treated with cycloheximide, as described previously (34). The mass ratio of polysome to monosome (P/M ratio) was measured from the A_{260} profile of the gradient samples. However, due to different abundance of the 60 S subunit, the P/M ratio here was calculated as the ratio of polysome abundance to the sum of the abundances of free 40 S, free 60 S, and the monosome. The P/M ratio was converted to the fraction of ribosomes found in polysome fractions by the formula $1/(1 + (1/a))$, where a is the P/M ratio.

To determine the mass ratio of 60 S to 40 S subunit (60 S/40 S ratio) independent of polysome profiling, yeast cell extracts were prepared in the absence of free Mg^{2+} and resolved by sucrose gradient velocity sedimentation followed by monitoring subunit abundance at A_{260}, as described previously (39). The 60 S/40 S ratio was converted to the fraction of the excessive 60 S subunit abundance compared with the mass of 60 S and 40 S subunits, which can form a stoichiometric 80 S couple (used in Fig. 3*A*). Assuming that the wild-type cells contain 1:1 stoichiometry of these subunits, this value was calculated as $(b - a)/(1 + b)$, where a and b are the 60 S/40 S mass ratios for the wild-type (= 2.16) and mutant strains, respectively. The 60 S/40 S ratio was also converted to the percentage of 40 S subunit reduced by each mutation compared with the 40 S subunit abundance in wild-type cells (used in Fig. 3*C*). This was calculated as $(1 - a/b) \times 100$, where a and b are the 60 S/40 S ratio for wild-type and mutant, respectively, assuming that the 60 S subunit abundance was unaltered.

To determine the RNA sequence of the ribosomes, rRNA was isolated by a hot phenol method (40) and used to perform reverse-transcriptase (RT)-directed PCR after DNase I treatment (DNase I removes any contaminating plasmid DNA). For RT-PCR, we used Access Quick™ RT-PCR system (Promega) and a pair of oligos, as listed in supplemental Table S1 and supplemental Fig. S1. The resulting cDNA product was used for sequencing.

To study the abundance of different PIC intermediates, cycloheximide-treated yeast culture was fixed with formaldehyde for preparing whole cell extracts, which are then resolved by sucrose gradient velocity sedimentation, as described previously (41). One-third of the gradient samples were precipitated with ethanol and analyzed with SDS-PAGE followed by immunoblotting with rabbit polyclonal anti-SUI2 (eIF2α) (42), -TIF5 (eIF5) (43), -TIF35 (eIF3g) (44), -SUI1 (eIF1) (45), -TIF11 (eIF1A) (46), -Rps0,[4] and mouse monoclonal anti-TIF32 (eIF3a) (47) antibodies.

[³H]Met-tRNA$_i^{Met}$ binding assay was performed in the presence of a nonhydrolyzable GTP analogue, GMPPNP, as described previously (48). 40 S subunit purification was performed also as described previously (48). To perform GST pulldown assays with the purified 40 S subunit, we purified GST-eIF1 and -eIF1A fusion proteins from *E. coli* BL21 derivatives bearing pGEX-SUI1 (36) and p3415 (46), respectively, and performed GST pulldown assays, as described with minor modifications (49). Briefly, the glutathione resin adsorbed with 5 μg of GST fusion proteins was blocked by preincubating with 100 μg/ml preheated total yeast tRNA (Sigma), and after washing the resin once with the binding buffer containing 100 mM KCl, the blocked resin-protein complex was incubated with two A_{260} units of purified 40 S subunit in the same binding buffer but with dry milk at 20 °C. Then the resin was washed three times with the binding buffer without dry milk and analyzed by SDS-PAGE, followed by immunoblotting with anti-RpsO antibodies.

Other Biochemical and Molecular Biology Methods—Standard molecular biology methods, including the β-galactosidase assay, were used throughout (34). To determine yeast titer on different agar plates, overnight culture was diluted to $A_{600} = 0.15$, and 5 μl of this and 10-fold serial dilutions were spotted, incubated under specified conditions, and photographed (34). The method of Northern blotting using PCR-generated ^{32}P-probe was also described (40). The ^{32}P-probe for 20 S, 23 S, and 35 S rRNA was generated by PCR with oligos 20 S-F and 20 S-R (supplemental Fig. S1 and supplemental Table S1), which were designed based on oligo probes previously used to detect 20 S rRNA with modifications (50, 51).

RESULTS

*Isolation of Point Mutations Altering Yeast rRNAs*—To understand the structure-function relationship of the eukary-

---

[4] L. Valášek, unpublished material.

otic ribosome in translation initiation, we attempted to isolate temperature-sensitive (Ts⁻) or slow growth (Slg⁻) mutations in yeast rRNA transcribed from an hc *LEU2* plasmid by random mutagenesis. We used the strain NOY890 (KAY488) deleted for all the chromosomal rDNA repeats (*rdn*ΔΔ) and instead carrying an hc *URA3* plasmid with a copy of *RDN* as the sole source of rRNA (30). Of >4000 clones, we obtained ~80 mutant candidates that showed Ts⁻ or Slg⁻ phenotypes after evicting the *URA3 RDN* helper plasmid using 5-fluoroorotic acid (FOA) as the drug to select against *URA3* (see "Materials and Methods"). We purified rDNA mutant plasmids from these candidates and reintroduced them to fresh NOY890 (KAY488), and the resulting transformants were subjected for growth on FOA-containing plates. ~30 FOA-resistant clones reproduced the growth phenotypes, suggesting that their phenotypes are due to mutations in the hc rDNA *LEU2* plasmid.

To find out if the isolated mutations compromise protein synthesis, we examined the polysome profile of all the mutants, grown at permissive (30 °C) and restrictive (36 °C) temperatures. Active translation of mRNA by multiple ribosomes results in formation of polysomes detected by sucrose gradient velocity sedimentation (34). 16 of the tested mutants substantially altered polysome profiles in two different ways. Type I, including nine mutants, initially designated *rdn-41* to *rdn-76* based on clone numbers, showed a strong accumulation of free 60 S subunit, with reduced polysome contents (see Fig. 2). Type II, including seven mutants, displayed a distinct polysome profile, with the decrease in free 60 S subunits and the appearance of half-mers (polysomes containing 40 S subunits awaiting 60 S subunit joining), which will be reported elsewhere.[5] Sequencing of the entire rDNA repeat from the 16 mutants (see "Materials and Methods") indicated that the type I mutations altered an 18 S rRNA base (supplemental Table S2), whereas the type II mutations changed a 25 S rRNA base. Because *rdn-41* and *rdn-59* also contained a mutation in 25 S rRNA (supplemental Table S2), we created yeast mutants just containing the 18 S rRNA mutations (called *rdn-41a* and *rdn-59a*, respectively) (Table 1) and confirmed that their polysome profile and growth defects are almost identical to those of the parental strains (supplemental Fig. S3, *A and B*, also see below). We also found that *rdn-63*, showing a weak Slg⁻ phenotype at 30 °C, had an insertion mutation in 18 S rRNA (Tables 1 and supplemental Table S1). Here, we report the characterization of the 10 mutants with altered 18 S rRNA (Table 1).

Most of the 18 S rRNA mutations (*rdn-41, -42, -44, -61, -71,* and *-76*) altered an evolutionarily conserved 18 S rRNA base (category 0 or 1, the highest or second highest degree of conservation, respectively, according to the 7-scale SSU RNA variability map), although *rdn-59, -60,* and *-72* altered a less conserved base (categories 3, 2, and 5, respectively) (*red arrows* in supplemental Fig. S2). In addition, we confirmed that the identified 18 S *rdn* mutations are different from naturally occurring base changes (polymorphisms) found in different strains or isolates of *S. cerevisiae* or its closely related species (*black arrows* in supplemental Fig. S2 and supplemental Table S4).
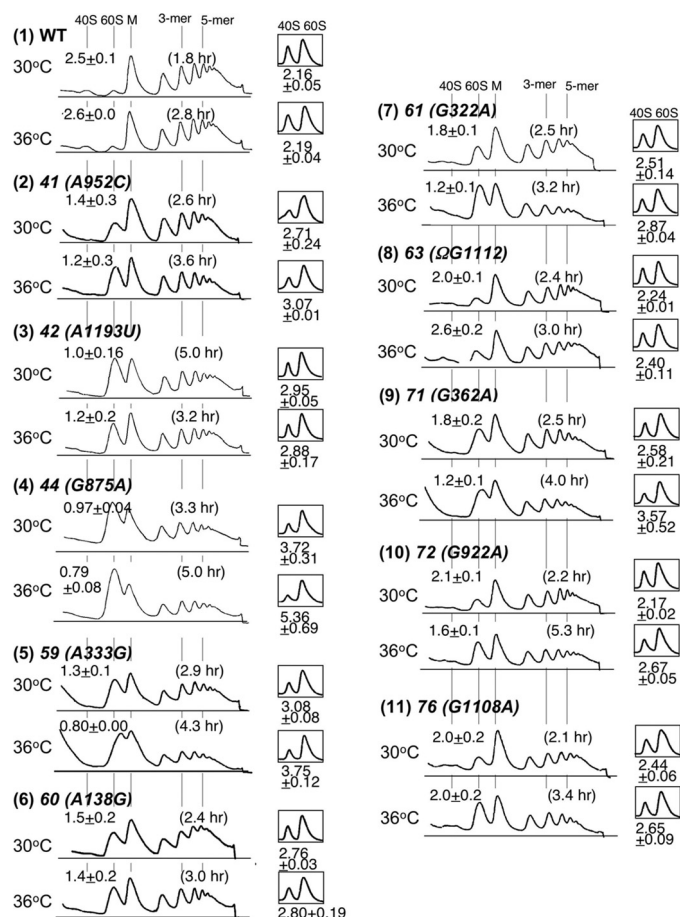
FIGURE 2. **Polysome profiles and 40 S/60 S subunit abundance ratio (*insets*) of the isolated 18 S rRNA mutants.** *Left columns* for each panel are as follows: A_{254} profiles of cell extracts prepared from wild-type and mutant yeasts (NOY908 derivatives in Table 1) that had been grown in the rich YPD medium at indicated temperatures for 3 h are shown with the P/M ratio and doubling time of the strains used (*n* = 2–4) (see "Materials and Methods"). *Lines* indicate the locations of free 40 S and 60 S subunits, monosomes (*M*), and polysomes with indicated number of ribosomes. *Right columns, insets* show A_{254} profile of total ribosomes dissociated into two subunits by the absence of Mg^{2+}. *Numbers below* indicate the mass ratio of 60 S to 40 S subunit, with *bars* indicating S.D. (*n* = 2–3). The original A_{254} profiles were traced by the autotrace function of the Canvas™ software.

To verify that the 18 S rRNA mutant yeast express the ribosomes with the corresponding mutations, the RNA samples isolated from the mutant yeast were treated with DNase I, to eliminate any contaminating plasmid DNAs, and then used for RT-PCR (see "Materials and Methods"). After confirming that the reaction generates cDNA in the presence of RT (supplemental Fig. S4A, lanes labeled +) but not in its absence (lanes labeled −), we determined the cDNA sequence around the mutation site. As shown in supplemental Fig. S4B, all of the cDNAs generated from the mutant 18 S rRNA contained the mutated nucleotide, confirming that the detectable majority of the ribosomes found in the *rdn* mutants is the expected mutant ribosome.

Because the analyses as described above indicated that the single 18 S rRNA base change identified was the cause of the phenotype related to protein synthesis, hereafter, we designate the individual 18 S *rdn* alleles with their base changes in 18 S rRNA. To relate this study to *Escherichia coli* ribosome, we also add the corresponding *E. coli* 16 S rRNA base number in paren-

TABLE 1

S. cerevisiae strains carrying *rdn* mutations and their phenotypes

Mutation	18 S rRNA base change	Altered domain	Helix altered	Subunit bridge affected[a]	Plasmid introduced	GCN2+ strains[b]	his4-306(TTG) strains[c]	Gcn[d]	Ssu[e]
WT	Wild-type				pNOY373	NOY908, KAY761	KAY165	+	+
rdn-41	A952C*	Central	22 bulge	B2e	pNOY373-41	KAY498, KAY757	KAY428	−	+
rdn-41a	A952C	Central	h22 bulge	B2e	pNOY373-41a	KAY906	NC	−	NT
rdn-42	A1193U	3'-Major	h31 loop		pNOY373-42	KAY767	KAY429	−	−
rdn-44	G875A	Central	h22 bulge	B2e	pNOY373-44	KAY776	KAY431	−	+
rdn-59	A333G*	5'	h11 loop	B4 and/or eB10	pNOY373-59	KAY575, KAY769	KAY449	−	+
rdn-59a	A333G	5'	h11 loop	B4 and/or eB10	pNOY373-59a	KAY907	NC	−	NT
rdn-60	A138G	5'	Junction of h7/10 and h8/9		pNOY373-60	KAY500, KAY778	KAY455	±	+
rdn-61	G322A	5'	h11 bulge	B4 and/or eB10	pNOY373-61	KAY501, KAY770	KAY450	±	+
rdn-63	ΩG1112	Central	h27 bulge		pNOY373-63	KAY502, KAY780	KAY451	±	+
rdn-71	G362A	5'	h12 stem		pNOY373-71	KAY546, KAY760	KAY462	±	+
rdn-72	G922A	Central	h23 stem	B2d/e	pNOY373-72	KAY547	KAY463	±	+
rdn-76	G1108A	Central	bottom of h27		pNOY373-76	KAY549, KAY768	KAY494	±	+

[a] Intersubunit bridges potentially affected, based on cryo-EM structures with subatomic resolutions (15–17), B, universally conserved bridge; eB, Eukarya-specific bridge.
[b] Derivatives of NOY908 (MATa *ade2-1 his3-11 leu2-3,112 ura3-1 trp1-1 can1-100 rdnΔΔ::HIS3* pNOY373 [2μ *RDN LEU2*]) carrying indicated mutations.
[c] Derivatives of KAY165 (MATa *ade2-1 his3-11 leu2-3,112 ura3-1 trp1-1 can1-100 rdnΔΔ::HIS3 his4-306(TTG)* pNOY373 [2μ *RDN LEU2*]) carrying indicated mutations. NC, not constructed for this study.
[d] Gcn phenotype as judged by the experiment in Fig. 5A. −, reduced viability as well as reduced colony growth in the presence of 3AT; ±, reduced colony growth only.
[e] Ssu phenotype as judged by the experiment in Fig. 5C. NT, not tested.

theses. Thus, *rdn-42* is designated *A1193U* (*A968*), etc. For *rdn-41* and *rdn-59* with additional mutations in 25 S rRNA, we designate the originally isolated alleles as *A952C** (*G742*) and *A333G** (*A262*), respectively, and we distinguish them from *A952C* (*G742*) and *A333G* (*A262*), which were created as *rdn-41a* and *rdn-59a*, respectively, as mentioned above.

Location of rdn Mutation Sites within the Predicted Structure of Yeast 18 S rRNA—Comparative genomics predicts that yeast 18 S rRNA consists of four domains as follows: 5′, central, 3′ major, and 3′ minor domains (Fig. 1*A*). Examination of the sites of the mutations within the proposed secondary structure of yeast 18 S rRNA indicated that all the mutations except *A1193U* (*A968*) changed a residue in the 5′ or central domain of 18 S rRNA. Specifically, *A138G* (*A143*), *G322A* (*G251*), *A333G* (*A262*), and *G362A* (*C290*) altered the 5′ domain, whereas *G875A* (*A663*), *A952C* (*G742*), *G922A* (*G711*), *G1108A* (*G885*), and Ω*G1112* (*G888*) mapped in the central domain (Fig. 1, *A* and *B*, shows bases corresponding to those in *E. coli* sequence). Cryo-EM structure of eukaryotic ribosomes (15–17) suggests that five of them directly disrupt a bridge to the 60 S subunit (Table 1, 5th column) and that other *rdn* mutations, as well as *A333G* (*A262*) (Fig. 1*A*), affect the 60 S subunit interface indirectly in part by disrupting A-minor interactions (*blue* and *red boxes* and *lines* in Fig. 1*A*) predicted from bacterial ribosome structure at atomic resolutions (see "Discussion").[6] These speculations provide a potential basis for phenotypes observed with the isolated mutations, as described below, but need to be justified in the future by x-ray structure of eukaryotic ribosomes at an atomic resolution.

A1193U (*A968*) is the only mutation found here to alter the 3′ major domain. The altered base in h31 loop locates directly below the codon-anticodon helix at the P-site (Fig. 1*C*). Mutations directly affecting yeast tRNA$_i^{Met}$ binding to the 40 S subunit have been mapped in a different helix, h28, of the 3′ major domain (31). Therefore, in addition to h28, the h31 loop appears to constitute tRNA$_i^{Met}$-binding site. This idea is further tested, as shown below.

18 S rRNA Mutants Contain Fewer 40 S Subunits than 60 S Subunits—As shown in Fig. 2, the 18 S *rdn* mutants show strong 60 S subunit accumulation in their polysome profiles. Agarose gel electrophoresis and ethidium bromide staining confirmed that the accumulated mass at the 60 S position of every mutant profile indeed contains 25 S rRNA with the correct size (data not shown). Thus, it was conceivable that a significant proportion of the mutant 40 S subunit was depleted by defective biogenesis or stability in each of the 18 S rRNA mutant strains. To confirm the depletion of 40 S subunits relative to 60 S subunits, we prepared the ribosome fractions in the absence of free Mg^{2+} and measured the relative abundance of 40 S and 60 S subunits

---

[6] *G362A* (*C290*) might disrupt the potential A-minor interaction with a helix in the central domain (denoted as "?" in Fig. 1*A*, as h21 does not possess an adenosine donor for this interaction). *G1108A* (*G885*) and Ω*G1112* (*G888*) alter residues at the foot of h27, connecting a structure tightly packed by at least three A-minor interactions (*blue boxes* and *lines* in Fig. 1*A*), which may bring the h27 loop and adjacent areas closer to the coaxially stacked 21/22/23 helix, forming B2c, B2d, B2e, and eB9. Finally, *A138G* (*A143*) changes a base connecting two coaxially stacked helices made of h7/10 and h8/9, potentially disrupting the structure of 5′ domain that constitutes the major interface to the 60 S subunit.

A

B

C
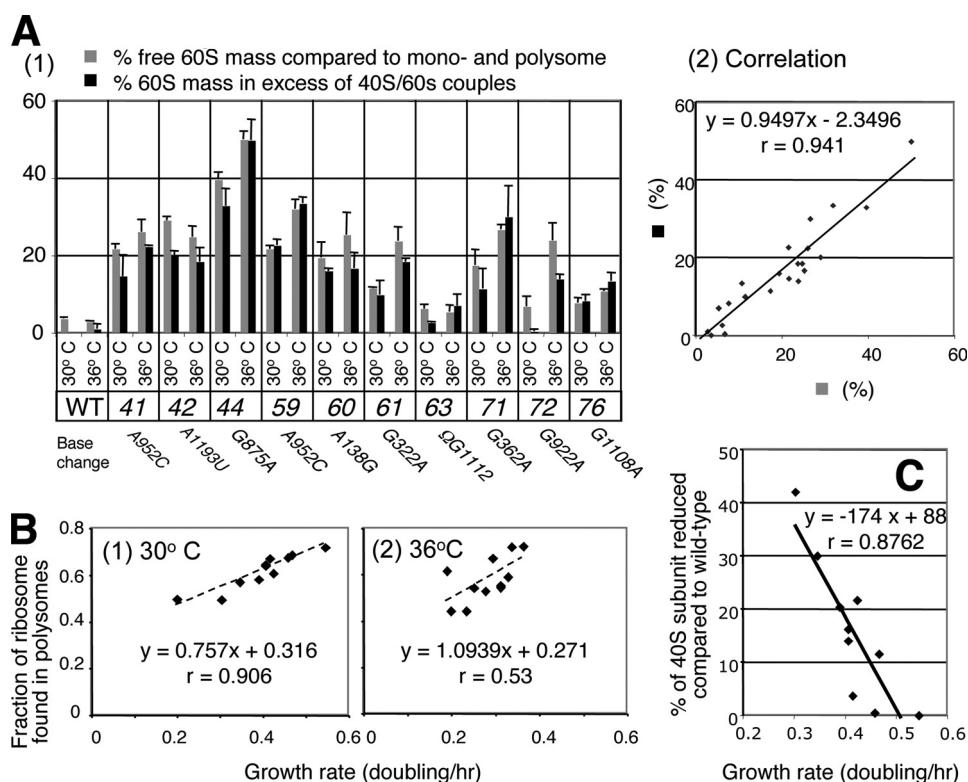
FIGURE 3. **Correlation studies.** *A, panel 1* indicates comparison of the level of free 60 S subunit found in polysomes (*gray bars*) with the level of 60 S subunit in excess of potential 40 S/60 S couples (*filled bars*, see "Materials and Methods"). The former was calculated as the mass ratio of free 60 S subunit to the sum of monosome and polysome, measured from polysome profiles in Fig. 2. *Bars* indicate S.D. (*n* = 2–4). *Panel 2* examines statistical correlation of these independently obtained values. *B*, relationship between the growth rate (doubling/h) and the fraction of ribosomes found in polysome fractions (see "Materials and Methods"). The data from cells grown at 30 and 36 °C were plotted separately in *panels 1* and *2*, respectively. *C*, relationship between the growth rate (doubling/h) and the percentage of 40 S subunit reduced compared with 40 S subunit abundance in wild-type cells. Data from growth at 30 °C was used, except for *A1193U* (*A968*). To evaluate the significance of the observed correlation, we used the command Regression under Data Analysis of Microsoft Excel.

by sucrose gradient analysis, independent of polysome profiling (see "Materials and Methods"). As shown in the *insets* of Fig. 2, *panel 1*, the 60 S/40 S ratio for wild-type, which would correspond to 1:1 stoichiometry of the subunits, was 2.16, comparable with previously reported values (52). The *insets* of other panels in Fig. 2 show that all the 18 S rRNA mutants contained a higher ratio of the 60 S subunit mass against the 40 S mass than the ratio for wild type (see supplemental Fig. S3A insets for reconstructed alleles, *A952C* and *A333G*). *rdn-63* or *ΩG1112* (*G888*) barely increased the 60 S/40 S ratio at 36 °C (Fig. 2, *panel 8*), qualifying this mutation as the weakest of "type I" polysome defect. These results confirm the depletion of the 40 S subunit in our Ts$^-$ or Slg$^-$ mutants.

To examine whether the observed reduction in 40 S subunit abundance can quantitatively account for the strong 60 S subunit accumulation in the 18 S rRNA mutant polysome profiles, we calculated the percentage of free 60 S subunit found in the polysome profiles (examples shown in Fig. 2) compared with the total ribosome mass in the profiles (*gray bars* in Fig. 3*A*, *panel 1*). As shown in Fig. 3*A*, these values correlate significantly (*r* = 0.941, *p* = 2.16 × e^{-10}, see *panel 2*) with the percentage of excessive 60 S subunit relative to the mass of the 40 S and 60 S subunits that can form a single ribosome (*filled bars* in *panel 1*), values obtained from the independent measurement

of 60 S/40 S ratio. Thus, the accumulation of free 60 S subunit observed in the mutant polysome profiles is largely due to the depletion of mutant 40 S subunits.

Extent of 40 S Subunit Depletion by 18 S rRNA Mutations Correlates with Decrease in Translation Initiation Rate—The polysome profiles in Fig. 2 also indicated that the polysome contents of most of the 18 S rRNA mutants, as measured by the ratio of polysome-to-monosome abundance (P/M), were lower than that of the wild-type *RDN* strain at permissive (30 °C) and restrictive (36 °C) temperatures, suggesting defects in translation initiation. The plot of the fraction of ribosomes found in polysome fractions (calculated from the P/M ratio) against the growth rate (times doubling/h) of each mutant indicates a linear correlation for the dataset measured at 30 °C (Fig. 3*B*, *panel 1*; *r* = 0.906, *p* = 0.0003), confirming that the decrease in cellular translation initiation resulted in a corresponding decrease in growth rate. We noted, however, that the growth at 36 °C disrupted this correlation (Fig. 3*B*, *panel 2*; *r* = 0.53, *p* = 0.11). We do not know the reason for this, but among many other possibilities, this may be because ribosomes defective in the elongation phase slow down the migration of translating ribosomes, thereby increasing the polysome abundance (34, 53).

We also found that the extent of 40 S subunit depletion, as calculated from 60 S/40 S abundance ratio, significantly correlated with decrease in the growth rate of each mutant at 30 °C (Fig. 3*C*; *r* = 0.876, *p* = 0.0019) if we eliminate the data from the *A1193U* (*A968*) mutant showing the most severe functional defect (see below). Thus, the 40 S subunit depletion by 18 S rRNA mutations directly resulted in a decrease in translation initiation rate. Our results also indicate that the 40 S subunit is a limiting component of translation initiation, as observed for essential yeast initiation factors (eIF1A, eIF4G1, and eIF4E) by their quantitative depletion studies (54).
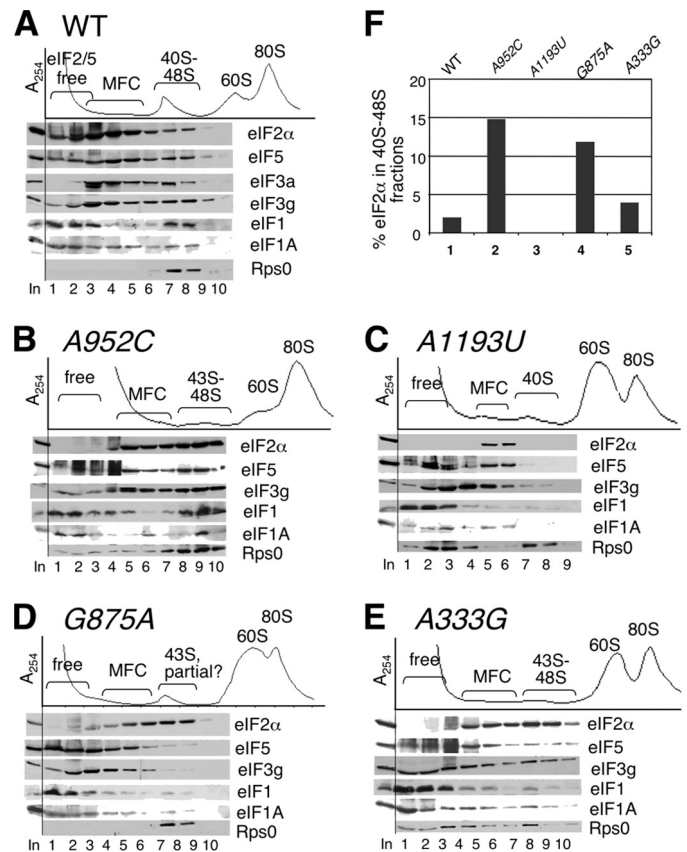
Processing of 18 S rRNA Appears to Be Normal in the 18 S rdn Mutants Except A1193U (A968)—In an effort to understand the mechanism whereby the 18 S *rdn* mutations reduce 40 S subunit abundance and translation initiation rate, we first examined the processing of 18 S rRNA in yeast strains bearing these mutations. During 18 S rRNA biogenesis, RNA polymerase I transcribes 35 S rRNA, whose 5′ external transcribed sequence is removed to generate the 32 S species by cleavages A$_0$ and A$_1$. 32 S rRNA is then cleaved at A$_2$ to generate 20 S rRNA. Finally, 20 S rRNA is transported to the cytoplasm, and

cleavage D eliminates its excess 3′ terminal sequence (supplemental Fig. S5*A*) (21). Cleavage A_3 not only is the first cleavage leading to the maturation of 5.8 S and 25 S rRNAs, but it also generates an aberrant 23 S species from the 5′-third of 35 S rRNA, which escaped A_0, A_1, and A_2 cleavages (50). Northern blot analyses using the probe specific to the region 3′ of 18 S (generated by PCR using oligos 20 S-F and 20 S-R in supplemental Table S1) indicated that no detectable 18 S biogenesis intermediates, such as 35 S, 20 S, or 23 S species, abnormally accumulated in the 18 S rRNA mutants (supplemental Fig. S5*B*, *panel 2*) except for *A1193U* (*A968*) with a buildup of 20 S prerRNA (supplemental Fig. S5*B*, *lanes 3* and *7*; see *panel 3* for quantification). We loaded RNA samples isolated from the same A_{600} units of the exponentially growing yeast culture. Therefore, the increase in 20 S rRNA observed by *A1193U* (*A968*) is most likely due to the increase in its steady-state abundance, although detailed analyses on its production rate are necessary to conclude this. The 20 S species increased by this mutation was not detected by EtBr staining (supplemental Fig. S5*B*, *panel 1*, *lanes 3* and *7*), and therefore its effect on ribosome function would be minimal. These results suggest that the processing of 18 S rRNA is normal in the *rdn* mutants except *A1193U* (*A968*) and that the reduced 40 S subunit abundance in these mutants are due to degradation of the final product, the 40 S subunit (also see "Discussion").

18 S rRNA Mutations Impair the Formation or Function of Productive PIC—To study the steady-state abundance of different initiation complex intermediates in *rdn* mutants, we fractionated formaldehyde-treated yeast extracts by sucrose gradient velocity sedimentation, and analyzed the gradient samples by immunoblotting for the PIC components, eIF1A, -1, -3, and -5, and the Rps0 subunit of the 40 S subunit (see "Materials and Methods"). We examined four strongest Ts⁻/Slg⁻ mutants, *A333G* (*A262*), *G875A* (*A663*), *A952C* (*G742*), and *A1193U* (*A968*), together with the *RDN⁺* control strain. As shown in Fig. 4*A*, free 40 S subunits found in the *RDN⁺* cells are loaded with up to ~5% of eIF2α, -3a, -3g, and -5 (see Fig. 4*F* for % of eIF2α found in free 40 S fraction). Given that these factors occur substoichiometrically to the 40 S subunit (molar ratio of 1 (eIF2):1 (eIF5):0.5 (eIF3):3 (40 S)) and that ~10% of 40 S subunit occur free of the 80 S ribosome (55), the majority (>75%) of the 40 S mass detected by A_{254} and anti-RpsO antibodies (Fig. 4*A*, *top* and *bottom*) is considered as 40 S subunits free of these eIFs, in agreement with previous observations (55). Fig. 4*A* also identified eIF complexes free of the 40 S subunits, including MFC (eIF1/2/3/5/tRNA$_i^{Met}$; *lanes 3–5*) (8, 56) and the eIF2/eIF5 complex free of Met-tRNA$_i^{Met}$ (*lanes 1–3*) (57).

Strikingly, *A1193U* (*A968*) impaired the MFC interaction with the 40 S subunit (Fig. 4*C*, *lanes 7* and *8*), allowing the former to accumulate at a significant level (*lanes 5* and *6*).[7] This

FIGURE 4. **Steady-state abundance of PIC and its intermediates *in vivo*.** *A–E*, PIC and its different intermediates found in NOY908 (*A*), KAY906 (*B*), KAY767 (*C*), KAY776 (*D*), and KAY907 (*E*) (Table 1) were analyzed by sucrose gradient velocity sedimentation, as described under "Materials and Methods." *Top*, A_{254} profile of gradient fractions. *Brackets*, deduced location of different eIF complexes. *Free*, free eIFs. *Bottom gels*, immunoblot patterns of one-third of the gradient samples from corresponding A_{254} profile with antibodies raised against proteins listed to the *right*. *Lane 1*, top of the gradient fraction. *In*, 1% in-put amount of extracts loaded on the gradient. Anti-Rps0 immunoblots for *B*, *C*, and *E* were exposed longer to indicate the location of 40 S-48 S fractions; *F*, graph indicates the amount of eIF2α found in 40 S-48 S fractions from each mutant.

---

[7] The RpsO-containing product smaller than 40 S was found in *A1193U* (*A968*) and *A333G* (*A262*) mutants (Fig. 4, *C* and *E*). This intermediate corresponds to only <1–2% of the total 40 S subunit and was observed by a longer exposure to show the diminished abundance of 40 S subunit. The abundance of the Rps0 product observed in *A1193U* likely reflects the destruction of the 40 S subunit with the most severe functional defect. Thus, we do not believe that the observation of these levels of the intermediate indicates a direct defect in the structure and composition of the pool of 40 S

agrees with the idea that A1193 is directly involved in tRNA$_i^{Met}$ binding. In contrast, other mutations increased the fraction of eIF2α bound to the 40 S subunit, even though they decreased the abundance of free 40 S subunit detected by A_{254} (Fig. 4, *B*, *D*, and *E*; see *F* for quantification of bound eIF2α). In the case of *A952C* (*G742*) altering h22, the majority of the 40 S subunit mass detected by A_{254} appears to be loaded with full PIC components (Fig. 4*B*, *lanes 8–10*), with ~5 times more eIF2α loaded onto the 40 S subunit than in wild type (Fig. 4*F*, *column 2*). The observed accumulation of the 43 S/48 S PIC suggests a defect in step(s) after 48 S complex assembly, including scanning or 60 S subunit joining (see below for its phenotype indicating defective initiation). In theory, the accumulation can be explained by the accelerated PIC assembly, but the Slg⁻ phenotype of the mutant may exclude this possibility.

In the case of *G875A* (*A663*) also altering h22, most of the free 40 S subunit seems to be bound with eIF2 only (partial 43 S complex) (Fig. 4*D*, *lanes 7* and *8*). The free 40 S subunit found in

---

subunits; this would be rather due to partial destruction in response to the 18 S rRNA functional defect.

A333G (*A262*) appears to be the mixture of the partial 43 S complex and the fully loaded PIC, because the relative abundance of eIF2α on the 40 S subunit seems to be greater than that of other PIC components (Fig. 4*E*, *lanes 8* and *9*).[7] Although the mechanism whereby the partial 43 S complex is formed requires further examination (see "Discussion"), the reduced amount of eIF1, -3, and -5 in the 40 S fractions suggests that *G875A* (*A663*) and *A333G* (*A262*) impair the interaction of MFC components (eIF1, -3, and -5) with the 40 S subunit. These results indicate that the amount of free 40 S subunit devoid of eIFs is greatly reduced in all the four *rdn* mutants examined, consistent with the limitation of free 40 S subunit available for initiation. Moreover, they suggest that the individual *rdn* mutations impair different steps of PIC formation or function.

Some 18 S rRNA Mutants Are Sensitive to Histidine Starvation Due to Altered AUG Recognition—To identify defects in specific steps of translation initiation *in vivo*, we took advantage of yeast general amino acid control pathway, which depends on the Gcn4p transcription factor (58). Translational control of *GCN4* in response to amino acid availability depends on upstream ORFs (uORFs) in the leader region (*schematics* at *top* of Fig. 5*B*). When amino acids are plentiful, special *cis*-elements around uORF1 allow the terminating ribosome to re-initiate translation of one of the downstream uORFs, thereby repressing translation of *GCN4*. When amino acids are limited, Gcn2 eIF2 kinase is activated to phosphorylate eIF2, thereby inhibiting eIF2B-catalyzed formation of active eIF2-GTP complex. This prevents a timely formation of the PIC prior to translation of the inhibitory uORFs, allowing translation of *GCN4*. Because of this mechanism of *GCN4* translational control, general amino acid control expression is, in some cases, a sensitive indicator of defects in translation initiation activities (59). For example, if a translation initiation mutation causes faulty recognition of the uORF1 start codon, this leads to failure to express *GCN4* under the amino acid starvation conditions. As a consequence, the mutant yeast cannot overcome growth inhibition caused by the starvation (general control nonderepressible or Gcn⁻ phenotype).

The drug 3-aminotriazole (3AT) is an inhibitor of His3p enzyme, causing histidine starvation. The growth of yeast in the presence of 3AT requires general amino acid control expression, and therefore, 3AT sensitivity conferred by a genetic mutation signifies a Gcn⁻ phenotype. As shown in Fig. 5*A*, *panel 3*, all the 18 S rRNA mutants are more or less sensitive to 50 mM 3AT at a semi-restrictive temperature of 34 °C, suggesting that they are Gcn⁻ (Table 1, column 9). Four of the strongest 18 S rRNA mutants, *A333G* (*A262*), *G875A* (*A663*), *A952C** (*G742*), and *A1193U* (*A968*) were even sensitive to a lower concentration of 3AT (30 mM) (Fig. 5*A*, *panel 2*, *rows 2–5*), suggesting that their Gcn⁻ phenotypes are stronger (also see Fig. 5*B*, below).[8]

---

[8] The Gcn⁻ phenotypes observed in Fig. 5*A* with the original constructs, *A333G** (*A262*) and *A952C** (*G742*) (each with a different 25 S mutation, see supplemental Table S2), were also observed with *A333G* (*A262*) and *A952C* (*G742*) carrying only the 18 S rRNA mutations (supplemental Fig. S3C).
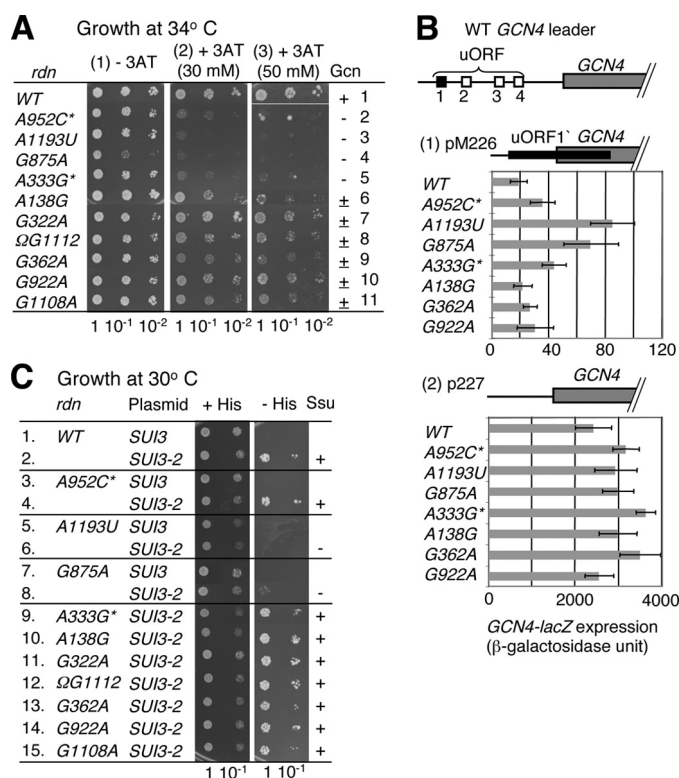
FIGURE 5. **Translation initiation phenotypes of 18 S *rdn* mutations.** *A*, test of Gcn⁻ phenotypes. Cultures of NOY908 (*GCN2⁺ rdnΔΔ*) derivatives bearing indicated mutations were diluted and spotted onto synthetic complete medium plates lacking histidine without (−*3AT*) or with (+*3AT*) the indicated concentrations of 3AT, and the plates were incubated for 4 (*panels 1* and *2*) and 7 (*panel 3*) days at 34 °C. *B*, *GCN4-lacZ* reporter assays. *Top*, structure of *GCN4* mRNA leader region, with *line* indicating mRNA, and *boxes* indicating reading frames (*filled box*, uORF1 required for *GCN4* translation re-initiation; *open boxes*, uORF2-4 to suppress *GCN4* translation; *gray box*, GCN4). *Panels 1* and *2* summarize β-galactosidase activities expressed from the reporter plasmid at 34 °C in transformants of NOY908 derivatives carrying *rdn* mutations listed to the *left* (Table 1, column 7). Schematics at the *top* of each panel depict the structure of modified *GCN4-lacZ* leader carried on the plasmid used. *Bars* indicate S.D. from >4 independent experiments. *C*, test of Ssu⁻ phenotypes. Cultures of transformants of KAY165 (*his3-306^UUG rdnΔΔ*) derivatives bearing indicated mutations (Table 1, column 8) carrying YCpU-SUI3 (*SUI3*) or -SUI3-2 (*SUI3-2*) (32) were diluted and spotted onto synthetic complete medium lacking uracil with (+*His*) or without (−*His*) histidine and incubated for 2 and 7 days, respectively, at 30 °C.

To investigate the mechanism underlying the observed Gcn⁻ phenotype, we measured β-galactosidase activities from *GCN4-lacZ* plasmid, pM226, in a select set of the 18 S rRNA mutants. The *GCN4-lacZ* allele in this plasmid is preceded by a modified uORF1 whose stop codon locates within *GCN4* reading frame (*schematics* in Fig. 5*B*, *panel 1*, *top*), which in turn strongly prevents translation of *GCN4-lacZ*. Thus, any increase in *GCN4-lacZ* expression compared with the value obtained with wild-type strain reflects the increased frequency of the bypass or "leaky scanning" of the uORF1 start codon. We found that two of the Gcn⁻ mutations, *A1193U* (*A968*) and *G875A* (*A663*), strongly, and *A952C** (*G742*) and *A333G** (*A262*) weakly but significantly, increased *GCN4-lacZ* expression from pM226 ($p < 0.01$, $n = 8$) at the semi-restrictive temperature of 34 °C (Fig. 5*B*, *panel 1*). As a control, *GCN4-lacZ* expression with no uORF preceding *GCN4* (p227) was increased only modestly (<1.5-fold) by the *rdn* mutations tested (Fig. 5*B*, *panel 2*), confirming that changes observed with pM226 were at the

translational level. Thus, the Gcn⁻ phenotypes of the *rdn* mutants likely occurred at least partially due to bypassing uORF1.

A1193U (A968) and G875A (A663) Impair Control of Stringent AUG Selection—To investigate more specific defects in stringent AUG selection *in vivo*, we used the *his4-306* allele with the AUG-to-UUG initiation codon mutation as a phenotypic reporter. *SUI3-2* mutation altering eIF2β reduces eIF2 interaction with tRNA$_i^{Met}$, thereby increasing the spontaneous release of eIF2 from the scanning ribosome (43). This increases the chance of initiating translation from the noncanonical UUG start codon, to suppress His⁻ phenotype of *his4-306*^{UUG} allele (suppressor of initiation codon mutation or Sui⁻ phenotype) (Fig. 5C, *rows 1* and *2*). As shown in Fig. 5C, *rows 5–8*, *A1193U* (*A968*) and *G875A* (*A663*) suppressed the ability of *SUI3-2* to express His4p from *his4-306* at 30 °C (Ssu⁻ or suppressor of *Su*i phenotype). *A1193U* (*A968*) alters the h31 loop, located below the P-site Met-tRNA$_i^{Met}$, whereas *G875A* (*A663*) changes h22, the core helix of the central domain, which is suggested to serve as the eIF platform. Thus, the mutant ribosome with an altered decoding site appears to be unable to mistakenly form a productive PIC on a UUG codon, even though *SUI3-2* mutation promotes eIF2 release from the PIC positioned at the UUG codon.

A1193U (A968) and G875A (A663) Are Defective in the Interaction with PIC Components in Vitro—Finally, we investigated whether A1193U (A968) and G875A (A663) directly impair integrity of the PIC by *in vitro* interaction assays. First, we purified mutant ribosomes and assayed their ability to promote [³H]Met-tRNA$_i^{Met}$ binding to the 40 S subunit in the wild-type yeast extracts. As shown in Fig. 6A, *solid line*, the addition of purified wild-type 40 S subunit increased [³H]Met-tRNA$_i^{Met}$ binding by 2.6 (+1.1, n = 4)-fold compared with the amount bound by the endogenous 40 S subunit. Importantly, 40 S subunits purified from *A1193U* (*A968*) and *G875A* (*A663*) strains were unable to promote the assembly, indicating defects in the interaction with Met-tRNA$_i^{Met}$. This defect observed with *A1193U* (*A968*) was as expected, because it alters a base potentially proximal to the P-site tRNA. This is also consistent with the analysis of PIC intermediates *in vivo* (Fig. 4C). In contrast, *G875A* (*A663*) does not directly alter the predicted Met-tRNA$_i^{Met}$-binding site. However, Met-tRNA$_i^{Met}$ is delivered to the 40 S subunit in the TC with the GTP-bound eIF2, which in turn binds to the 40 S subunit in the context of MFC made with eIF1, -3, and -5 (8, 60). Thus, we hypothesize that *G875A* (*A663*) disrupts a critical interface to the MFC components, eIF1 or eIF3, in particular, as they are suggested to directly bind the 40 S subunit. Again, this is consistent with the observation of partial 43 S complex (the 43 S PIC lacking eIF1, -3, and -5) in the *G875A* (*A663*) mutant (Fig. 4D; also see under "Discussion").

To directly test if *A1193U* (*A968*) and *G875A* (*A663*) are defective in the interaction with eIF1 and eIF1A, we performed GST pulldown assays. The 40 S subunits purified from *RDN*⁺ and *G875A* (*A663*) bound efficiently to GST-eIF1 or -eIF1A (Fig. 6B). However, *A1193U* (*A968*) altering the h31 loop reduced the interaction with both GST-eIF1 and -eIF1A (Fig. 6B, *panel 3*), suggesting that the conformation of the P-site is important for the small factors to bind near the decoding site. In
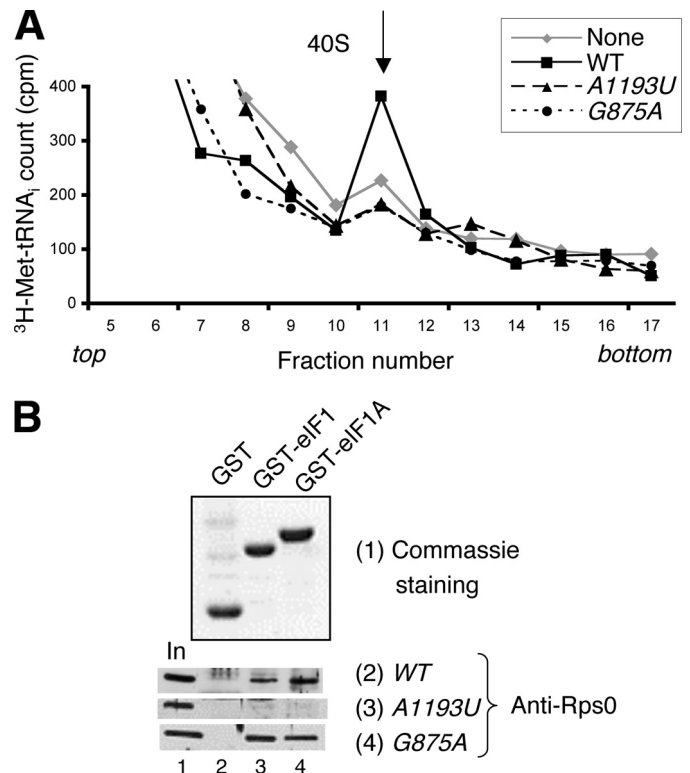
FIGURE 6. ***A1193U* (*A968*) and *G875A* (*A663*) impair the interaction with the PIC components *in vitro*.** *A*, cell-free translation extracts were prepared from NOY908 and supplemented with [³H]Met-tRNA$_i^{Met}$, together with purified wild-type (*WT*) or *rdn* mutant 40 S subunits at 1.0 A_{260} unit, which is comparable with the amount of free 40 S subunit observed by sucrose gradient analysis of the cell extracts. The reaction mixture was fractionated by sucrose gradient velocity sedimentation, and gradient samples were analyzed by scintillation counting. ³H counts in relevant fractions are shown with an *arrow* indicating the fraction containing free 40 S subunit. *B*, GST or GST fusion proteins listed across the top (see *panel 1* for their Coomassie staining patterns) were allowed to bind the 40 S subunit from either wild-type (*WT*, *panel 1*), *A1193U* (*A968*) (*panel 2*), or *G875A* (*A663*) (*panel 3*). The 40 S subunit co-precipitated was detected by anti-Rps0 antibodies (see "Materials and Methods"). *In*, 40% in-put amount of the 40 S subunit.

agreement with this finding, *A1193U* (*A968*) severely impaired eIF1 and eIF1A loading to the 40 S subunit (Fig. 4C). In conclusion, the data presented here together suggest strongly that 18 S rRNA structure around the decoding site and the eIF platform is crucial for the integrity of the scanning PIC and the control of stringent AUG selection.

DISCUSSION

Here we identified, using yeast genetic screening, 10 new residues of yeast 18 S rRNA important for its function and/or maintenance. Not surprisingly, from reduced 40 S subunit abundance observed with the 18 S rRNA mutants (Fig. 2), the primary consequence of these mutations was to compromise the initiation, rather than elongation, phase of translation. Accordingly, these mutations led to strong accumulation of free 60 S subunit in the polysome profile characterized as type I (Fig. 2), and this effect directly led to slower growth rate (Fig. 3C). 60 S subunit accumulation has been observed in previous site-directed mutagenesis studies on 18 S rRNA (26), but here it became clear that the depletion of 40 S subunit is a general consequence of mutations altering 18 S rRNA (also see below).

Role of Yeast 18 S rRNA in Translation Initiation

A1193U (A968) and G875A (A663) Directly Impair Regulation of Start Codon Selection by the PIC—We found that at least two of the strongest *rdn* mutations directly impair the 40 S subunit function in regulating start codon selection. *A1193U* (*A968*) and *G875A* (*A663*) increased the frequency of leaky scanning an AUG codon (Fig. 5*B*). We also provided genetic evidence suggesting that *A1193U* (*A968*) and *G875A* (*A663*) prevented the PIC on a UUG codon from maturing into the 40 S IC due to weak interaction between eIF2 and tRNA$_i^{Met}$ (Fig. 5*C*). Biochemical evidence is presented that *A1193U* (*A968*) impairs the interaction with TC, eIF1A, and eIF1 (Fig. 6), thereby disrupting the integrity of the PIC *in vivo* (Fig. 4*C*). Therefore, it is conceivable that the h31 loop close to the P-site, altered by *A1193U* (*A968*), indeed interacts with Met-tRNA$_i^{Met}$ during the scanning process and that the defective interaction leads to bypassing a start codon, regardless of whether it was correct or incorrect.

As for the h22 altered by *G875A* (*A663*), this is not only a part of the core helix structure (h21/22/23) of the 40 S subunit platform domain but is also predicted to constitute a universally conserved bridge to the 60 S subunit termed Bridge 2e (B2e) (also see Table 1, column 5) (15–17). *In vivo*, G875A (A663) impaired the PIC formation, allowing accumulation of the partial 43 S complex containing only eIF2 (Fig. 4*D*). Although eIF3 binds the solvent side of the 40 S subunit, the eIF1/3/5 complex together can cover a significant portion of the interface side, including the intersubunit bridges (19). Disruption of B2e or the platform/body structure by *G875A* (*A663*) can affect the interaction with the eIF1/3/5 complex, such that this interaction cannot tolerate fractionation by sucrose gradient velocity sedimentation. Alternatively, the h22 mutation might have prevented the 43 S PIC formation via MFC, thereby allowing TC alone to bind the 40 S subunit. This model is consistent with the slower TC binding to the 40 S subunit bearing the same mutation observed in yeast extracts (Fig. 6*A*), because TC binding in the absence of MFC is expected to be slow. The h22 is also altered by *A952C* (*G742*), another Gcn$^-$ mutation (Fig. 5, *A* and *B*; supplemental Fig. S3), which introduces an additional base pair to the same bulge of h22 altered by *G875A* (*A663*) (Fig. 1*A*). Together with the Ssu$^-$ phenotype observed with *G875A* (*A663*) (Fig. 5*C*), this study highlights the importance of the h22 during the initiation function and, perhaps, the conformational change of the 40 S subunit in response to AUG selection.

Effect of rRNA Mutations on General Control Response—We showed that mutations in 18 S rRNA can impair general control response (Gcn$^-$ phenotype) in part due to leaky scanning of uORF1 in the *GCN4* mRNA leader (Fig. 5). This is not the consequence of depleting 40 S subunits observed with these mutations (Fig. 2), because a strong depletion of the 40 S subunits (2-fold increase in 60 S/40 S ratio compared with wild-type) caused by the deletion of *RP51* encoding a small ribosomal protein does not cause Gcn$^-$ phenotype (61). In agreement with strong leaky scanning observed with *A1193U* (*A968*) and *G875A* (*A663*) (Fig. 5*B*), Dong *et al.* (31) showed that point mutations disrupting h28 increased leaky scanning of uORF1 and uORF4, the positive and negative regulatory elements for *GCN4* translation, respectively.

Remarkably, however, some of the Dong *et al.* (31) mutations, *e.g. A1152U* (*A928*), were isolated as mutations that increase *GCN4* expression independent of Gcn2 eIF2 kinase (General control derepressed or Gcd$^-$). Because the leaky scanning of uORF1 impairs *GCN4* translation and attendant general control response (3AT sensitivity or Gcn$^-$ phenotype), as observed here in Fig. 5*A*, the constitutive *GCN4* translation by these mutations must be due to an additional mechanism. Indeed, Dong *et al.* (31) showed that the Gcd$^-$ mutations were suppressible by overproduction of eIF2 TC *in vivo* and impair TC loading to the 40 S subunit *in vitro* (31). Together with our findings (Fig. 5*A*), these results indicate that 18 S rRNA mutations altering P-site (h28 or h31) impair TC loading as well as post-assembly function in scanning or AUG selection. It is also noteworthy that the deletion of *RPL16b* encoding a large ribosomal protein has long been known to display a weak Gcd$^-$ phenotype and a modest leaky scanning of uORF4 (61). In contrast to our 18 S rRNA mutations, this deletion mutation leads to the depletion of the 60 S subunit. Thus, the phenotypes observed with *rpl16b* deletion would be solely due to the defect in 60 S subunit joining, which apparently allowed even the committed (wild type) 40 S subunit to bypass uORFs 2–4, the negative regulatory elements. This suggests that the 40 S subunit commitment to form 80 S initiation complex in response to AUG selection is canceled by the absence of the 60 S subunit after a certain time. More work involving thorough mutagenesis of 18 S and 25 S rRNAs is needed to fully understand the role of the ribosome structure and function in gene regulation, including uORF-mediated translational control of *GCN4*.

Relationship between Functional Defect and Stability of the Mutant 40 S Subunits—*A1193U* (*A968*) altering the h31 loop would likely affect the modification of Ψ 1191, located two bases away from A1193. The lack of Ψ 1191 modification due to the small nucleolar RNA mutation causes a cold-sensitive Slg$^-$ phenotype and accumulation of free 60 S subunit in the polysome profile and of 20 S species (62), all as observed with *A1193U* (*A968*) (this mutant grows slowly at 30 °C but not at 36 °C, consistent with a cold-sensitive growth, as shown in Fig. 2, *panel 3*). However, *A1193U* (*A968*) apparently confers a stronger Slg$^-$ phenotype than a strain defective in Ψ 1191 modification, so *A1193U* (*A968*) would directly impair the 40 S subunit function, rather than doing so via defective modification of the neighboring base.

Although the possible defect in Ψ 1191 modification may explain 40 S subunit depletion by *A1193U* (*A968*), the mechanism leading to reduced 40 S subunit abundance in other 18 S *rdn* mutants remains unclear. However, because we did not observe any change in 18 S rRNA intermediates except for *A1193U* (*A968*) (supplemental Fig. S5) and because all of the 10 18 S rRNA mutations conferred sensitivity to 3AT by a mechanism likely involving defective *GCN4* translation (Fig. 5), it could be hypothesized that the functional defect of each mutant 40 S subunit led to a corresponding degree of its cytoplasmic degradation. That all the mutations except *A1193U* (*A968*) alter the body (5′) and platform (central) domains, which together include the major 60 S interface, is consistent with the idea that defective 60 S subunit joining can trigger such degradation (23, 24). On the other hand, we observed the accumula-

tion of vacant monosomes in the polysome profiles of all the mutants (Fig. 2); thus, the *rdn* mutant 40 S subunits appear to able to form vacant ribosomes efficiently, and therefore, their selective degradation may not be explained by the failure to form vacant, inactive ribosomes.

Based on the data presented here, we suggest among other possibilities that most of the individual 18 S mutations disrupt intersubunit bridges directly or indirectly (see Table 1, column 5).[6] This not only leads to defective 60 S subunit joining at the last step of initiation, potentially leading to selective degradation of the mutant 40 S subunit, but also results in defective formation of scanning-competent PIC. This is consistent with the idea that eIF1, -1A, -2, and -5, which govern the fidelity of start codon recognition, bind the 60 S subunit interface of the 40 S subunit (19). There is currently little information on the role of individual bridges in stabilizing subunit association, nor is it known which bridges are sequestered by eIFs for anti-association. Mutational studies of 18 S rRNA bases around some of the strong *rdn* mutations identified here would provide a profitable direction to be explored in the future.

REFERENCES

1. Hinnebusch, A. G., Dever, T. E., and Asano, K. (2007) in *Translational Control in Biology and Medicine* (Mathews, M. B., Sonenberg, N., and Hershey, J. W., eds) pp. 225–268, Cold Spring Harbor Laboratory Press, Cold Spring Harbor, NY
2. Noller, H. F. (2007) in *Translational Control in Biology and Medicine* (Mathews, M. B., Sonenberg, N., and Hershey, J. W., eds) pp. 41–58, Cold Spring Harbor Laboratory Press, Cold Spring Harbor, NY
3. Pestova, T. V., Lorsch, J. R., and Hellen, C. U. (2007) in *Translational Control in Biology and Medicine* (Mathews, M. B., Sonenberg, N., and Hershey, J. W., eds) pp. 87–128, Cold Spring Harbor Laboratory Press, Cold Spring Harbor, NY
4. Roll-Mecak, A., Shin, B. S., Dever, T. E., and Burley, S. K. (2001) *Trends Biochem. Sci.* **26,** 705–709
5. Allen, G. S., and Frank, J. (2007) *Mol. Microbiol.* **63,** 941–950
6. Passmore, L. A., Schmeing, T. M., Maag, D., Applefield, D. J., Acker, M. G., Algire, M. A., Lorsch, J. R., and Ramakrishnan, V. (2007) *Mol. Cell* **26,** 41–50
7. Saini, A. K., Nanda, J. S., Lorsch, J. R., and Hinnebusch, A. G. (2010) *Genes Dev.* **24,** 97–110
8. Asano, K., Clayton, J., Shalev, A., and Hinnebusch, A. G. (2000) *Genes Dev.* **14,** 2534–2546
9. Algire, M. A., Maag, D., and Lorsch, J. R. (2005) *Mol. Cell* **20,** 251–262
10. Hasenöhrl, D., Fabbretti, A., Londei, P., Gualerzi, C. O., and Bläsi, U. (2009) *RNA* **15,** 2288–2298
11. Woese, C. R., Kandler, O., and Wheelis, M. L. (1990) *Proc. Natl. Acad. Sci. U.S.A.* **87,** 4576–4579
12. Noller, H. F. (2005) *Science* **309,** 1508–1514
13. Wimberly, B. T., Brodersen, D. E., Clemons, W. M., Jr., Morgan-Warren, R. J., Carter, A. P., Vonrhein, C., Hartsch, T., and Ramakrishnan, V. (2000) *Nature* **407,** 327–339
14. Gerbi, S. A. (1996) in *Ribosomal RNA: Structure, Evolution, Processing, and Function in Protein Synthesis* (Zimmermann, R. A., and Dahlberg, A. E., eds) pp. 71–87, CRC Press, New York
15. Spahn, C. M., Beckmann, R., Eswar, N., Penczek, P. A., Sali, A., Blobel, G.,

16. and Frank, J. (2001) *Cell* **107,** 373–386
16. Spahn, C. M., Gomez-Lorenzo, M. G., Grassucci, R. A., Jørgensen, R., Andersen, G. R., Beckmann, R., Penczek, P. A., Ballesta, J. P., and Frank, J. (2004) *EMBO J.* **23,** 1008–1019
17. Chandramouli, P., Topf, M., Ménétret, J. F., Eswar, N., Cannone, J. J., Gutell, R. R., Sali, A., and Akey, C. W. (2008) *Structure* **16,** 535–548
18. Taylor, D. J., Devkota, B., Huang, A. D., Topf, M., Narayanan, E., Sali, A., Harvey, S. C., and Frank, J. (2009) *Structure* **17,** 1591–1604
19. Asano, K., and Sachs, M. S. (2007) *Genes Dev.* **21,** 1280–1287
20. Lomakin, I. B., Kolupaeva, V. G., Marintchev, A., Wagner, G., and Pestova, T. V. (2003) *Genes Dev.* **17,** 2786–2797
21. Hage, A. E., and Tollervey, D. (2004) *RNA Biol.* **1,** 10–15
22. LaRiviere, F. J., Cole, S. E., Ferullo, D. J., and Moore, M. J. (2006) *Mol. Cell* **24,** 619–626
23. Fujii, K., Kitabatake, M., Sakata, T., Miyata, A., and Ohno, M. (2009) *Genes Dev.* **23,** 963–974
24. Cole, S. E., LaRiviere, F. J., Merrikh, C. N., and Moore, M. J. (2009) *Mol. Cell* **34,** 440–450
25. Chernoff, Y. O., Vincent, A., and Liebman, S. W. (1994) *EMBO J.* **13,** 906–913
26. Velichutina, I. V., Dresios, J., Hong, J. Y., Li, C., Mankin, A., Synetos, D., and Liebman, S. W. (2000) *RNA* **6,** 1174–1184
27. Konstantinidis, T. C., Patsoukis, N., Georgiou, C. D., and Synetos, D. (2006) *Biochemistry* **45,** 3525–3533
28. Tselika, S., Konstantinidis, T. C., and Synetos, D. (2008) *Biochimie* **90,** 908–917
29. Venema, J., Dirks-Mulder, A., Faber, A. W., and Raué, H. A. (1995) *Yeast* **11,** 145–156
30. Wai, H. H., Vu, L., Oakes, M., and Nomura, M. (2000) *Nucleic Acids Res.* **28,** 3524–3534
31. Dong, J., Nanda, J. S., Rahman, H., Pruitt, M. R., Shin, B. S., Wong, C. M., Lorsch, J. R., and Hinnebusch, A. G. (2008) *Genes Dev.* **22,** 2242–2255
32. Watanabe, R., Murai, M. J., Singh, C. R., Fox, S., Ii, M., and Asano, K. (2010) *J. Biol. Chem.* **285,** 21922–21933
33. Grant, C. M., Miller, P. F., and Hinnebusch, A. G. (1994) *Mol. Cell. Biol.* **14,** 2616–2628
34. Singh, C. R., and Asano, K. (2007) *Methods Enzymol.* **429,** 139–161
35. Boeke, J. D., Trueheart, J., Natsoulis, G., and Fink, G. R. (1987) *Methods Enzymol.* **154,** 164–175
36. Asano, K., Phan, L., Anderson, J., and Hinnebusch, A. G. (1998) *J. Biol. Chem.* **273,** 18573–18585
37. Van de Peer, Y., Jansen, J., De Rijk, P., and De Wachter, R. (1997) *Nucleic Acids Res.* **25,** 111–116
38. Wuyts, J., De Rijk, P., Van de Peer, Y., Winkelmans, T., and De Wachter, R. (2001) *Nucleic Acids Res.* **29,** 175–177
39. Decatur, W. A., Liang, X. H., Piekna-Przybylska, D., and Fournier, M. J. (2007) *Methods Enzymol.* **425,** 283–316
40. Udagawa, T., Nemoto, N., Wilkinson, C. R., Narashimhan, J., Jiang, L., Watt, S., Zook, A., Jones, N., Wek, R. C., Bähler, J., and Asano, K. (2008) *J. Biol. Chem.* **283,** 22063–22075
41. Reibarkh, M., Yamamoto, Y., Singh, C. R., del Rio, F., Fahmy, A., Lee, B., Luna, R. E., Ii, M., Wagner, G., and Asano, K. (2008) *J. Biol. Chem.* **283,** 1094–1103
42. Yang, R., Wek, S. A., and Wek, R. C. (2000) *Mol. Cell. Biol.* **20,** 2706–2717
43. Huang, H. K., Yoon, H., Hannig, E. M., and Donahue, T. F. (1997) *Genes Dev.* **11,** 2396–2413
44. Phan, L., Schoenfeld, L. W., Valásek, L., Nielsen, K. H., and Hinnebusch, A. G. (2001) *EMBO J.* **20,** 2954–2965
45. He, H., von der Haar, T., Singh, R. C., Ii, M., Li, B., Hinnebusch, A. G., McCarthy, J. E. G., and Asano, K. (2003) *Mol. Cell. Biol.* **23,** 5431–5445
46. Olsen, D. S., Savner, E. M., Mathew, A., Zhang, F., Krishnamoorthy, T., Phan, L., and Hinnebusch, A. G. (2003) *EMBO J.* **22,** 193–204
47. Jirincová, H., Vavricková, P., Palecek, J., and Hasek, J. (1998) *Folia Biol. (Praha)* **44,** 73
48. Asano, K., Phan, L., Krishnamoorthy, T., Pavitt, G. D., Gomez, E., Hannig, E. M., Nika, J., Donahue, T. F., Huang, H. K., and Hinnebusch, A. G. (2002) *Methods Enzymol.* **351,** 221–247
49. Singh, C. R., and Asano, K. (2007) *Methods Enzymol.* **429,** 139–161

50. Kressler, D., de la Cruz, J., Rojo, M., and Linder, P. (1997) *Mol. Cell. Biol.* **17,** 7283–7294

51. Vanrobays, E., Gleizes, P. E., Bousquet-Antonelli, C., Noaillac-Depeyre, J., Caizergues-Ferrer, M., and Gélugne, J. P. (2001) *EMBO J.* **20,** 4204–4213

52. Valásek, L., Hasek, J., Nielsen, K. H., and Hinnebusch, A. G. (2001) *J. Biol. Chem.* **276,** 43351–43360

53. Ortiz, P. A., and Kinzy, T. G. (2005) *Nucleic Acids Res.* **33,** 5740–5748

54. Sangthong, P., Hughes, J., and McCarthy, J. E. (2007) *Nucleic Acids Res.* **35,** 3573–3580

55. Singh, C. R., Udagawa, T., Lee, B., Wassink, S., He, H., Yamamoto, Y., Anderson, J. T., Pavitt, G. D., and Asano, K. (2007) *J. Mol. Biol.* **370,** 315–330

56. Singh, C. R., He, H., Ii, M., Yamamoto, Y., and Asano, K. (2004) *J. Biol. Chem.* **279,** 31910–31920

57. Singh, C. R., Lee, B., Udagawa, T., Mohammad-Qureshi, S. S., Yamamoto, Y., Pavitt, G. D., and Asano, K. (2006) *EMBO J.* **25,** 4537–4546

58. Hinnebusch, A. G. (2005) *Annu. Rev. Microbiol.* **59,** 407–450

59. Hinnebusch, A. G. (1997) *J. Biol. Chem.* **272,** 21661–21664

60. Yamamoto, Y., Singh, C. R., Marintchev, A., Hall, N. S., Hannig, E. M., Wagner, G., and Asano, K. (2005) *Proc. Natl. Acad. Sci. U.S.A.* **102,** 16164–16169

61. Foiani, M., Cigan, A. M., Paddon, C. J., Harashima, S., and Hinnebusch, A. G. (1991) *Mol. Cell. Biol.* **11,** 3203–3216

62. Liang, X. H., Liu, Q., and Fournier, M. J. (2009) *RNA* **15,** 1716–1728